

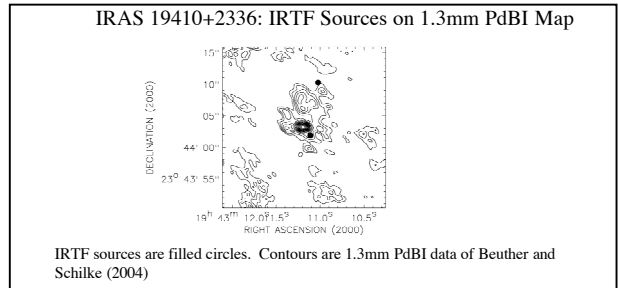
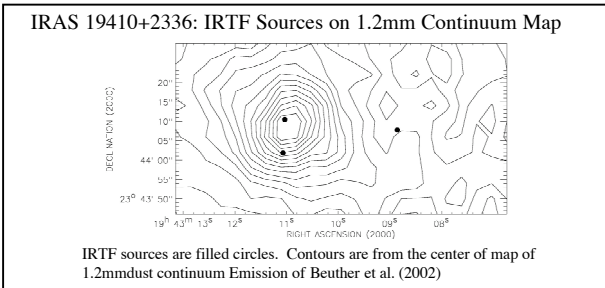
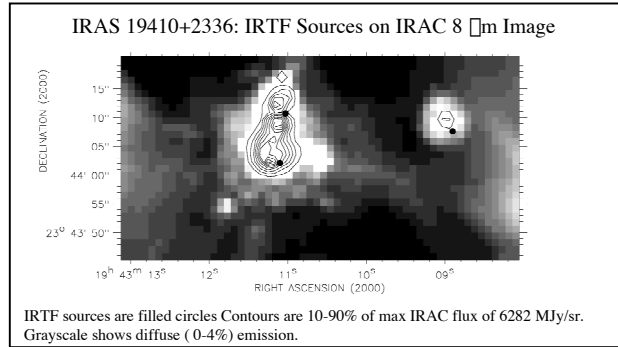
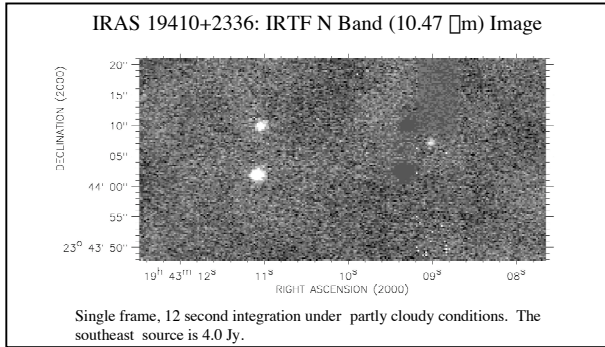
Compact Mid-IR Emission from High-Mass Protostellar Candidates

M. F. Campbell¹, T. K. Sridharan^{2,5}, H. Beuther², J. Hora^{2,5}, M. Kassir^{3,5}, J. D. Adams^{4,5}, S. H. Fung¹
¹ Colby College, Waterville, ME, USA ² SAO, Cambridge, MA, USA ³ Keck Obs., Kamuela HI, USA ⁴ Cornell Univ., Ithaca, NY, USA
⁵ Visiting Astronomer at the Infrared Telescope Facility, which is operated by the University of Hawaii under Cooperative Agreement no. NCC 5-538 with the National Aeronautics and Space Administration, Office of Space Science, Planetary Astronomy Program.

ABSTRACT: We observed 23 fields for High-Mass Protostellar Objects (HMPOs) at the IRTF in N band (10.47 μ m). 26 sources were detected in 18 fields. Most sources are compact, and they emit a significant fraction of the flux seen in the larger beam of the MSX telescope. The N band fluxes appear to correlate with the bolometric luminosities of the regions. Many N band sources peak near the 1.2mm continuum peak emission, so they appear to be preferentially located near the centers of each star-forming core. They appear to be individual HMPOs.

- Fields containing candidate HMPOs were chosen from a sample of 69 bright far-ir objects that have IRAS $F_{\lambda}(60 \mu\text{m}) > 90 \text{ Jy}$ and $F_{\lambda}(100 \mu\text{m}) > 500 \text{ Jy}$, IRAS colors indicative of high mass star formation, known molecular line emission, and low-level cm continuum emission (Sridharan, et al. 2002). The fields observed on the IRTF were chosen for bright, compact emission in MSX Band C (12.1 μ m).
- 26 objects were detected in N band (10.47 μ m) in 18 of 23 fields observed with MIRSI on the IRTF.

Example: IRAS 19410+2336 IRTF Image Compared to GLIMPSE Spitzer IRAC Image and mm Dust Continuum Maps



- Most sources are compact—near the IRTF diffraction limit of 0.9".
- The fields each contain only 1-3 sources,
 - Estimated 10 σ detection limits vary from 0.05 - 1.0 Jy.
 - IRTF positions in this survey are estimated to be uncertain to about 5".
- For IRAS 19410+2336, the IRAC 8 μ m image from the GLIMPSE database shows shifts in peak locations, suggestions of some fainter sources, and extended emission. It confirms the prominence of the bright point sources. Note, however, that the N band relative positions come from a single frame of the MIRSI array.
- IRTF sources account for large fractions of the mid-ir flux observed by the 18.1" beam MSX telescope. For the brightest source in each field, the average ratio of IRTF N band (10.47 μ m) F_{λ} to MSX Band C (12.1 μ m) F_{λ} is 0.38.

- Within broad limits (\pm factor of 10), the IRTF N band fluxes are proportional to bolometric fluxes based on IRAS SEDs derived from luminosities given by Sridharan et al. (2002). The relatively weaker N band sources are probably more deeply embedded in their natal clouds.
- Many IRTF N band positions are near peaks in 1.2mm continuum emission from cool dust presented by Beuther et al. (2002).
- The importance of high resolution mm continuum maps for understanding each region's structure is shown by the 1.3 mm PdBI map of IRAS 19410+2336 in comparison both to the single dish 1.2 mm map and to the mid-ir images.
- The IRTF N band sources are apparently due to circumstellar dust emission around the brightest HMPOs or high-mass young stellar objects in each field. The HMPOs appear to be preferentially located near the center of each star-forming cloud clump or protocluster.

APPENDIX. IRTF N BAND (10.47 μ m) OBSERVATIONS AND COMPARISONS

IRAS Source	IRTF Source	F_{λ} Jy N Band	F_{λ} Jy MSX F _λ (12.1)	IRTF F_{λ} (N) MSX F _λ (12.1)	IRTF-1.2mm Separation, mly	cm F_{ν}	2MASS K _s Obj. Within 5"	IRAS Source	IRTF Source	F_{λ} Jy N Band	F_{λ} Jy MSX F _λ (12.1)	IRTF F_{λ} (N) MSX F _λ (12.1)	IRTF-1.2mm Separation, mly	cm F_{ν}	2MASS K _s Obj. Within 5"
05338+3543	1	0.81	8.7	0.16	14	<1	yes	18530+0215	1	7.26	76.1	0.35	3	311.00	yes
	2	0.10	1.1	0.02	6	yes	yes	18533+0414	1	3.33	21.1	0.59	3	<1	no
05553+1631	1	0.46	5.7	0.24	5	1.30	yes	19410+2336	1	3.95	26.1	0.44	8	1.00	no
18089-1732	2	0.05	0.7	0.03	11	yes	yes		2	1.59	10.5	0.17	2	no	no
	1	0.51	7.5	0.20	8	0.90	yes		3	1.27	2.1	0.14	N/A	no	no
	2	0.26	3.9	0.10	8	yes	yes	20216+4107	1	4.62	4.7	0.58	4	1.40	yes
18151-1208	1	11.16	224.8	0.53	1	<1	yes	20343+4129	1	8.10	113.0	0.44	16	1.80	yes
18223-1243	1	0.93	9.9	0.08	12	<1	yes		2	3.74	52.1	0.20	3	yes	yes
18247-1147	1	5.17	17.0	0.57	4	47.00	yes		3	0.22	3.1	0.01	21	no	no
18337-0743	1	0.68	5.4	0.10	14	<1	yes	22134+5834	1	3.94	9.6	0.30	9	3.70	no
18348-0616	1	5.80	52.8	0.77	N/A	54.00	yes		2	2.07	5.0	0.16	11	no	no
18472-0022	1	3.83	5.4	1.27	N/A	194.00	no	22570+5912	1	0.57	2.0	0.05	3	29.00	yes
	2	0.63	0.9	0.21	24	yes	yes	23033+5951	1	3.22	13.6	0.57	9	1.70	yes
							no	23151+5912	1	22.10	20.3	0.44	2	<1	yes

Fields with non-detections in N band: 18445-0222, 18566+0408, 20293+3952, 20332+4124, 21391+5802

References: Beuther, H. et al. 2002 ApJ 566, 945 Beuther, H. & Schilke, P. 2004 Science 303, 1167 Sridharan, T. K. et al. 2002 ApJ 566, 933
 Acknowledgement: Thanks to Dr. John Kuehne for computer support at Colby College.